Journal of Marine Science and Technology

Volume 25 | Issue 1 Article 9

STUDY ON INS/DR INTEGRATION NAVIGATION SYSTEM USING EKF/RK4 ALGORITHM FOR UNDERWATER GLIDERS

Haoqian Huang
School of Instrument Science and Engineering, Southeast University, Nanjing, PR China.

Xiyuan Chen
School of Instrument Science and Engineering, Southeast University, Nanjing, PR China., chxiyuan@seu.edu.cn

Zhikai Zhou
School of Instrument Science and Engineering, Southeast University, Nanjing, PR China.

Hu Liu
School of Instrument Science and Engineering, Southeast University, Nanjing, PR China.

Caiping Lv
School of Instrument Science and Engineering, Southeast University, Nanjing, PR China.

STUDY ON INS/DR INTEGRATION NAVIGATION SYSTEM USING EKF/RK4 ALGORITHM FOR UNDERWATER GLIDERS

Acknowledgements

This work is supported by Natural Science Foundation of Jiangsu Province (No. BK20160699), Jiangsu Planned Projects for Postdoctoral Research Funds (No. 1601155C), Fundamental Research Funds for the Central universities (No. 2242016R20024), Public Science and Technology Research Funds Projects of Ocean (No. 201205035).

Journal of Marine Science and Technology, Vol. 25, No. 1, pp. 84-95 (2017)
DOI: 10.6119/JMST-016-0913-3

STUDY ON INS/DR INTEGRATION NAVIGATION SYSTEM USING EKF/RK$_4$ ALGORITHM FOR UNDERWATER GLIDERS

Haoqian Huang, Xiyuan Chen, Zhikai Zhou, Hu Liu, and Caiping Lv

Key words: inertial navigation system (INS), dead reckoning (DR), extended Kalman filter (EKF), Runge-Kutta (RK$_4$).

ABSTRACT

The underwater glider has the advantages of low power, long endurance and high accuracy. Micro-Electro-Mechanical-System (MEMS) grade inertial sensors are more suitable for an underwater glider because of their low cost and small size. Models of MEMS sensor noises which include not only the white noises and random walk terms but also the bias instabilities of the sensor noises are analyzed. The integrated navigation system for the underwater glider is composed of a dead reckoning (DR) module, an inertial navigation system (INS) based on MEMS sensors aided by a tri-axis magnetic sensor. Due to the inherent error characteristics, MEMS grade devices suffer from the non-stationary stochastic sensor errors and nonlinear inertial errors which cannot be well handled by the conventional filter algorithms, this paper proposes extended Kalman filter (EKF) fusing Runge-Kutta (RK$_4$) algorithm (EKF/RK$_4$) which can implement the data fusion of multisensor. The proposed EKF/RK$_4$ can take advantage of the EKF to achieve the optimal estimation of attitude and position and then make better use of the RK$_4$ to further improve the estimation accuracy. In order to evaluate the effectiveness of the proposed algorithm, the EKF/RK$_4$ algorithm is applied to the underwater navigation system designed in our lab and a series of land experiments are performed. The performance of the proposed EKF/RK$_4$ algorithm based on our navigation system is analyzed and compared with the traditional algorithms. The experiment results show that the proposed algorithm is more effective in reducing the attitude and position errors than KF/RK$_4$ and EKF.

Paper submitted 11/10/14; revised 02/15/16; accepted 09/13/16. Author for correspondence: Xiyuan Chen (e-mail: chxiyuan@seu.edu.cn).
School of Instrument Science and Engineering, Southeast University, Nanjing, PR China.

I. INTRODUCTION

As the development of science and technology processes, people are beginning to explore more and more fields. Autonomous underwater vehicles (AUVs) have become an interesting area of oceanic research because of their promising uses in homeland security, military applications, hydrographic surveys, environment monitoring, mineral field surveys and oceanographic studies. Over the years, there have been intensive efforts toward the development of sea-worthy AUVs to meet the challenges of exploitation programs and oceanographic exploration. Nowadays, the development of AUV is focused on improving the endurance and operation range for long term data collection in the fields of coastal management and oceanography (Kondoa and Ura, 2004; Tang et al., 2011; Zhu and Zhao, 2011; Sun et al., 2013 ; Alam et al., 2014).

Autonomous underwater gliders (AUGs) are a recently developed class of AUV driven by buoyancy changes to fly along saw-tooth trajectories through the ocean (Eriksen et al., 2001). Gliders quickly have attracted increasing attention with the longer range and higher endurance than AUV. The underwater navigation which can provide high accuracy navigation information for a long period of time has been a key technology for the wide application of AUG currently.

Navigation sensors usually include Inertial Navigation System (INS), Global Positioning System (GPS) receiver, Doppler Velocity Log (DVL), acoustic altimeter, etc. (Li et al., 2011; Chen et al., 2013). GPS, as a mature technology, can be used in the navigation and positioning field. It is capable of providing accurate position and velocity information. However, in order to provide accurate measurements, GPS needs at least four satellites with good geometry. There must be a direct line-of-sight between the GPS antennas and those satellites (Semeniuk and Noureldin, 2006; Jwo et al., 2010). GPS signal can not be received in deep seawater because of the Faraday cage effect of water for the radio-frequency signal (Li et al., 2011).

INS can give accurate attitude and position information for a short time period (Lee et al., 2007). Besides, advances of INS based on MEMS (Micro-Electro-Mechanical-System) have led to significant developments in low-cost inertial technology in the

last decade (Shen et al., 2010). It is improving (reductions in size, sensitivity and weight) and becoming cheaper due to mass productions (Bijker and Steyn, 2008; Chiang et al., 2012). Therefore, INS can be used as a main navigation sensor when GPS is unavailable. The errors of INS, however, increase with time elapse due to the inherent biases of gyroscopes and accelerometers. The errors will accumulate as time goes on and it needs additional sensors to compensate attitude and position errors of the INS (Chen et al., 2013; Chiang et al., 2013). Standard components such as the compass effectively suppress the attitude and position drift of INS (Hegrenæs and Hallingstad, 2011), but the effect achieved by only compass is limited. The dead reckoning (DR) is used to correct the outputs of INS, so the INS/DR integrated navigation method can improve the attitude and position accuracy greatly.

In addition to the navigation method, the data filtering algorithm play an important role in dealing with the problem of underwater navigation. The standard Kalman filter (KF) assumes that the system model has been fully characterized and the noise processes known statistical properties, which are often not satisfied in practical applications. The performance of the standard KF could be greatly degraded when the concerned system has model uncertainties and non-Gaussian noises (Kandepu et al., 2008; Cao and Guo, 2012). However, in the extended Kalman filter (EKF), the probability distribution function (pdf) is propagated through a linear approximation of the system around the operating point at each time instant. In order to perform the EKF analysis, one needs the Jacobian matrices which may be difficult to obtain for the higher order, especially in the case of time-critical applications. Furthermore, the linear approximation of the system at a given time instant may introduce errors in the state and it may lead to divergence of the state over time (Jwo and Cho, 2010; Wang and Huang, 2011; Chu et al., 2013). To overcome the drawbacks of the EKF, other nonlinear state estimators have been developed such as the unscented Kalman filter (UKF). The UKF seems to be a promising alternative for process control applications. The UKF propagates pdf in a simple and effective way and it is accurate up to the second order in estimating mean and covariance. Nevertheless, UKF costs more computing time than EKF in calculating the statistics of random variables that undergoes the nonlinear transformation. This filtering method is more suitable for measurements with Gaussian distribution, which is not always offered by MEMS-grade sensors (Stancić and Graovac, 2010; Shen et al., 2011). In the literature (Frogerais, et al., 2012), two methodologies to approximate the CD-EKF (continuous-discrete EKF) in general cases are presented. The first one uses deterministic scheme to integrate the differential moment equations (Joseph and LaViola, 2003; Mazzoni, 2007). The mean and the covariance can be recursively approximated by an explicit RungeKutta method. The second one introduces a discretediscrete EKF filter on a discrete version of the stochastic differential (Wilkie, 2004; Singer, 2005) to obtain a discrete approximation of the SDE (Stochastic Differential Equation) by the stochastic RungeKutta scheme. The main differences and novelties between our work and the methods mentioned in this above reference are not only the different subject studied but also the way to integrate RK_4 with EKF to estimate the navigation information optimally. A novel method which fuses the RK_4 into EKF frame (EKF/RK_4) is proposed in our paper from another perspective to solve the problem of navigation calculation for the multi-sensor data. The RK_4 is used to determine the state prediction estimate and subsequently EKF is performed to estimate other parameters of the navigation calculation. Therefore, the computation effectiveness and information estimation accuracy are improved greatly.

In this paper, we design a kind of underwater navigation system which has advantages of low power, simple design, high navigation accuracy and long endurance, and propose a more effective EKF/RK_4 algorithm for the underwater navigation system. The noise models of the inertial sensors are analyzed in Section 2 followed by the overall INS/DR integrated navigation scheme given in Section 3. The main aspects of the integration algorithm are proposed in detail in Section 4. Results and discussion of experimental verification of the system are presented in Section 5. Some conclusions are derived in Section 6.

II. ERROR MODELS ANALYSIS

1. Noise Model

Like any other physical sensor, both gyroscopes and accelerometers suffer from measurement errors. For these sensors, however, the error sources are multiple and are also coupled. Therefore, the sensor calibration is a non-trivial task (Aydemir and Saranlı, 2012).

The gyroscope outputs $\boldsymbol{\omega}_m$ are expressed as

$$\boldsymbol{\omega}_m = \boldsymbol{\omega} + \mathbf{B}_g + \boldsymbol{\eta}_g \tag{1}$$

where $\boldsymbol{\omega} = \begin{bmatrix} \omega_x & \omega_y & \omega_z \end{bmatrix}^T$ is the vector of true angular rates measured in the body fixed reference frame; $\mathbf{B}_g$ is the gyroscope noise bias vector; $\boldsymbol{\eta}_g$ is the angular random walk vector. Each component of the gyroscope noise bias

$$\mathbf{B}_g = \begin{bmatrix} B_{gx} & B_{gy} & B_{gz} \end{bmatrix}^T \tag{2}$$

is modeled as a sum of two components including bias instability and rate random walk (Grewal et al., 2007; Petkov and Slavov, 2010), so that

$$B_{gx} = x_1 + x_2,\ B_{gy} = x_3 + x_4,\ B_{gz} = x_5 + x_6 \tag{3}$$

where $x_1, x_2, x_3, x_4, x_5, x_6$ are states of the following differential equation matrix.

$$\begin{bmatrix}\dot{x}_1\\ \dot{x}_2\\ \dot{x}_3\\ \dot{x}_4\\ \dot{x}_5\\ \dot{x}_6\end{bmatrix}=\begin{bmatrix}-\frac{1}{T_g} & 0 & 0 & 0 & 0 & 0\\ 0 & 0 & 0 & 0 & 0 & 0\\ 0 & 0 & -\frac{1}{T_g} & 0 & 0 & 0\\ 0 & 0 & 0 & 0 & 0 & 0\\ 0 & 0 & 0 & 0 & -\frac{1}{T_g} & 0\\ 0 & 0 & 0 & 0 & 0 & 0\end{bmatrix}\begin{bmatrix}x_1\\ x_2\\ x_3\\ x_4\\ x_5\\ x_6\end{bmatrix}$$
$$+\begin{bmatrix}\frac{K_{g_1}}{T_g} & 0 & 0 & 0 & 0 & 0\\ 0 & K_{g_2} & 0 & 0 & 0 & 0\\ 0 & 0 & \frac{K_{g_1}}{T_g} & 0 & 0 & 0\\ 0 & 0 & 0 & K_{g_2} & 0 & 0\\ 0 & 0 & 0 & 0 & \frac{K_{g_1}}{T_g} & 0\\ 0 & 0 & 0 & 0 & 0 & K_{g_2}\end{bmatrix}\begin{bmatrix}w_{g_1}\\ w_{g_2}\\ w_{g_4}\\ w_{g_5}\\ w_{g_7}\\ w_{g_8}\end{bmatrix} \tag{4}$$

T_g is a time constant, K_{g_1}, K_{g_2} are constants and w_{g_1}, w_{g_2}, w_{g_4}, w_{g_5}, w_{g_7}, w_{g_8} are white noises with unit variances.

The angular random walk vector is given by

$$\boldsymbol{\eta}_g=\begin{bmatrix}\eta_{gx}\\ \eta_{gy}\\ \eta_{gz}\end{bmatrix}=\begin{bmatrix}K_{g_3}w_{g_3}\\ K_{g_3}w_{g_6}\\ K_{g_3}w_{g_9}\end{bmatrix} \tag{5}$$

where K_{g_3} is a constant and w_{g_3}, w_{g_6}, w_{g_9} are white noises with unit variances.

In a similar way the measured specific acceleration $\mathbf{a}_m$ is determined as

$$\mathbf{a}_m=\mathbf{a}_s+\mathbf{B}_a+\boldsymbol{\eta}_a \tag{6}$$

where $\mathbf{a}_s=\begin{bmatrix}a_x & a_y & a_z\end{bmatrix}^T$ is the specific acceleration; $\mathbf{B}_a$ is the vector of three-axis accelerometer bias; $\boldsymbol{\eta}_a$ is the vector of velocity random walk. Each component of the accelerometer bias $\mathbf{B}_a=\begin{bmatrix}B_{ax} & B_{ay} & B_{az}\end{bmatrix}^T$ is expressed as a sum of bias instability and acceleration random walk.

$$B_{ax}=x_7+x_8,\ B_{ay}=x_9+x_{10},\ B_{az}=x_{11}+x_{12} \tag{7}$$

where x_7, x_8, x_9, x_{10}, x_{11}, x_{12} are states of the differential equation matrix.

$$\begin{bmatrix}\dot{x}_7\\ \dot{x}_8\\ \dot{x}_9\\ \dot{x}_{10}\\ \dot{x}_{11}\\ \dot{x}_{12}\end{bmatrix}=\begin{bmatrix}-\frac{1}{T_a} & 0 & 0 & 0 & 0 & 0\\ 0 & 0 & 0 & 0 & 0 & 0\\ 0 & 0 & -\frac{1}{T_a} & 0 & 0 & 0\\ 0 & 0 & 0 & 0 & 0 & 0\\ 0 & 0 & 0 & 0 & -\frac{1}{T_a} & 0\\ 0 & 0 & 0 & 0 & 0 & 0\end{bmatrix}\begin{bmatrix}x_7\\ x_8\\ x_9\\ x_{10}\\ x_{11}\\ x_{12}\end{bmatrix}$$
$$+\begin{bmatrix}\frac{K_{a_1}}{T_a} & 0 & 0 & 0 & 0 & 0\\ 0 & K_{a_2} & 0 & 0 & 0 & 0\\ 0 & 0 & \frac{K_{a_1}}{T_a} & 0 & 0 & 0\\ 0 & 0 & 0 & K_{a_2} & 0 & 0\\ 0 & 0 & 0 & 0 & \frac{K_{a_1}}{T_a} & 0\\ 0 & 0 & 0 & 0 & 0 & K_{a_2}\end{bmatrix}\begin{bmatrix}w_{a_1}\\ w_{a_2}\\ w_{a_4}\\ w_{a_5}\\ w_{a_7}\\ w_{a_8}\end{bmatrix} \tag{8}$$

T_a is a time constant, K_{a_1}, K_{a_2} are constants, and w_{a_1}, w_{a_2}, w_{a_4}, w_{a_5}, w_{a_7}, w_{a_8} are white noises with unit variances.

The velocity random walk vector is determined from

$$\boldsymbol{\eta}_a=\begin{bmatrix}\eta_{ax}\\ \eta_{ay}\\ \eta_{az}\end{bmatrix}=\begin{bmatrix}K_{a_3}w_{a_3}\\ K_{a_3}w_{a_6}\\ K_{a_3}w_{a_9}\end{bmatrix} \tag{9}$$

where K_{a_3} is a constant, and w_{a_3}, w_{a_6}, w_{a_9} are white noises with unit variances (Slavov and Petkov, 2011).

2. Error Model in State Space

The phi-angle position, velocity, and attitude errors are given below (Stancić and Graovac, 2010; Zhang and Xu, 2012; Jwo et al., 2014).

Phi-angle error is given by:

$$\dot{\boldsymbol{\phi}}^n=\delta\boldsymbol{\omega}_{ie}^n+\delta\boldsymbol{\omega}_{en}^n-(\boldsymbol{\omega}_{ie}^n+\boldsymbol{\omega}_{en}^n)\times\boldsymbol{\phi}^n-\mathbf{B}_g^n \tag{10}$$

where $\boldsymbol{\phi}^n=\begin{bmatrix}\phi_E & \phi_N & \phi_U\end{bmatrix}^T$ is the orientation error of the cal-

culated platform represented in the local East-North-Upward (ENU) coordinate frame; $\boldsymbol{\omega}_{ie}^{n}=\begin{bmatrix}0 & \omega_{ie}\cos L & \omega_{ie}\sin L\end{bmatrix}^{T}$ represents the rotation projections of the Earth onto the ENU axes; ω_{ie} = 7.292115 × 10^{-5} rad/s represents the angular velocity of the rotation of the Earth; $\boldsymbol{\omega}_{en}^{n}=\begin{bmatrix}-\dfrac{V_N}{R_n+h} & \dfrac{V_E}{R_e+h} & \dfrac{V_E\tan L}{R_e+h}\end{bmatrix}^{T}$ represents the angular velocity of the rotation of a navigation coordinate frame relative to Earth; $\delta\boldsymbol{\omega}_{ie}^{n}$, $\delta\boldsymbol{\omega}_{en}^{n}$ represent the slow variances of $\boldsymbol{\omega}_{ie}^{n}$, $\boldsymbol{\omega}_{en}^{n}$ respectively; λ, L, h represent the position coordinates (longitude, latitude and height, respectively); R_n, R_e represent the radii of the curvatures along the meridian and parallel, respectively.

Velocity error is given by (Grewal and Andrews, 2008):

$$\begin{aligned}\delta\dot{\mathbf{V}}^{n}=&\mathbf{f}^{n}\times\boldsymbol{\phi}^{n}+\mathbf{B}_{a}^{n}-(2\delta\boldsymbol{\omega}_{ie}^{n}+\delta\boldsymbol{\omega}_{en}^{n})\\&\times\dot{\mathbf{V}}^{n}-(2\boldsymbol{\omega}_{ie}^{n}+\boldsymbol{\omega}_{en}^{n})\times\delta\mathbf{V}^{n}\end{aligned}\tag{11}$$

where $\delta\mathbf{V}^{n}=\begin{bmatrix}\delta V_E & \delta V_N & \delta V_U\end{bmatrix}^{T}$ represents the linear velocity errors; $\mathbf{f}^{n}=\begin{bmatrix}f_E & f_N & f_U\end{bmatrix}^{T}$ represents the specific force vector, therefore, the velocity errors equations in ENU axes are as follows:

$$\begin{aligned}\delta\dot{V}_E=&\phi_U f_N-\phi_N f_U+\delta V_E\frac{V_N\tan L-V_U}{R_e+h}\\&+\delta V_N\left(2\omega_{ie}\sin L+\frac{V_E}{R_e+h}\tan L\right)\\&-\delta V_U\left(2\omega_{ie}\cos L+\frac{V_E}{R_e+h}\right)\\&+\delta L\left[2\omega_{ie}(V_U\sin L+V_N\cos L)+\frac{V_E V_N}{R_e+h}\sec^2 L\right]\\&+\delta h\frac{V_E V_U-V_E V_N\tan L}{(R_e+h)^2}+B_{aE}\end{aligned}$$

$$\begin{aligned}\delta\dot{V}_N=&-\phi_U f_E+\phi_E f_U-\delta V_E\left(2\omega_{ie}\sin L+\frac{2V_E}{R_e+h}\tan L\right)\\&-\delta V_N\frac{V_U}{R_n+h}-\delta V_U\frac{V_N}{R_n+h}\\&-\delta L\left(2V_E\omega_{ie}\cos L+V_N\cos L+\frac{V_E^2}{R_e+h}\sec^2 L\right)\\&+\delta h\left[\frac{V_N V_U}{(R_e+h)^2}+\frac{V_E^2\tan L}{(R_e+h)^2}\right]+B_{aN}\end{aligned}$$

$$\begin{aligned}\delta\dot{V}_U=&\phi_N f_E-\phi_E f_N+\delta V_E\left(2\omega_{ie}\cos L+\frac{2V_E}{R_e+h}\right)\\&+\delta V_N\frac{2V_N}{R_n+h}-\delta L\bullet 2V_E\omega_{ie}\sin L\\&-\delta h\left[\frac{V_N^2}{(R_n+h)^2}+\frac{V_E^2}{(R_e+h)^2}\right]+B_{aU}\end{aligned}\tag{12}$$

The attitude errors equations in ENU axes are as follows:

$$\begin{aligned}\dot{\phi}_E=&\phi_N\left(\omega_{ie}\sin L+\frac{V_E}{R_e+h}\tan L\right)-\phi_U\left(\omega_{ie}\cos L+\frac{V_E}{R_e+h}\right)\\&-\frac{\delta V_N}{R_n+h}+\delta h\frac{V_N}{(R_n+h)^2}-B_{gE}\end{aligned}$$

$$\begin{aligned}\dot{\phi}_N=&-\phi_E\left(\omega_{ie}\sin L+\frac{V_E}{R_e+h}\tan L\right)\\&-\phi_U\frac{\delta V_N}{R_n+h}-\delta L\omega_{ie}\sin L\\&+\frac{\delta V_E}{R_e+h}+\delta h\frac{V_E}{(R_e+h)^2}-B_{gN}\end{aligned}$$

$$\begin{aligned}\dot{\phi}_U=&\phi_E\left(\omega_{ie}\cos L+\frac{V_E}{R_e+h}\right)+\phi_N\frac{V_N}{R_n+h}\\&+\delta L\left(\omega_{ie}\cos L+\frac{\delta V_E}{R_e+h}\sec^2 L\right)\\&+\frac{\delta V_E}{R_e+h}\tan L-B_{gU}\end{aligned}\tag{13}$$

where $\mathbf{B}_{a}^{n}=\begin{bmatrix}B_{aE} & B_{aN} & B_{aU}\end{bmatrix}^{T}=\mathbf{C}_{b}^{n}\bullet\begin{bmatrix}B_{ax} & B_{ay} & B_{az}\end{bmatrix}^{T}$ represents the biases of the accelerometer projections onto the ENU axes; moreover, B_{aE} = 0, B_{aN} = 0, B_{aU} = 0. B_{ax}, B_{ay}, B_{ay} represent the biases of the accelerometers in the body coordinates, respectively; $\mathbf{C}_{b}^{n}$ represents the attitude matrix which gives relationship between vectors in the body fixed reference frame and the corresponding vectors in the Earth fixed reference frame; $\mathbf{B}_{g}^{n}=\begin{bmatrix}B_{gE} & B_{gN} & B_{gU}\end{bmatrix}^{T}=\mathbf{C}_{b}^{n}\bullet\begin{bmatrix}B_{gx} & B_{gy} & B_{gz}\end{bmatrix}^{T}$ represents the gyroscope drift projections onto the ENU axes; moreover, $\dot{B}_{gE}=0$, $\dot{B}_{gN}=0$, $\dot{B}_{gU}=0$. B_{gx}, B_{gy}, B_{gz} represent the drifts of the gyroscope in the body coordinates.

The position errors equations in ENU axes are as follows:

$$\begin{aligned}\delta\dot{L}&=\frac{\delta V_N}{R_n+h}-\delta h\frac{V_N}{(R_n+h)^2}\\\delta\dot{\lambda}&=\frac{\delta V_E}{R_e+h}\sec L+\delta L\frac{V_E}{R_e+h}\tan L\sec L-\delta h\frac{V_E\sec L}{(R_e+h)^2}\\\delta\dot{h}&=\delta V_U\end{aligned}\tag{14}$$

III. NAVIGATION SYSTEM STRUCTURE

1. DR Model

The three dimension model of gliding is shown in Fig. 1. It is analyzed in this paper that the glider gliders stably in the sea. When the glider glides at certain depth in the sea, the circum-

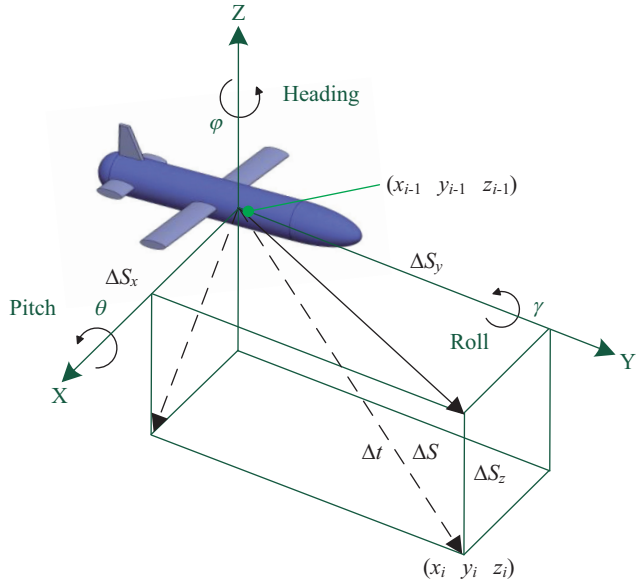

Fig. 1. The three dimension model of glider.

stance of underwater is comparatively stable. The glider usually follows a sawtooth motion pattern in the vertical plane and progresses along a straight line or piecewise line in the horizontal plane (Zhang et al., 2013). The change of depth is measured by the depthometer or other instruments, and it may be not the focus in this paper. The acquisition of navigation information mainly by the inertial system in the horizontal plane is studied in the following content. Here, the dynamic model of glider is simplified properly according to some analyses for underwater gliders in the reference (Asher et al., 2008; Hussain et al., 2011; Zhang et al., 2013). The sea current average velocity is approximately regarded as a constant in the certain depth and the glider glides with the sea current. Hence, the average velocity of glider is also considered as a constant.

Assume that the glider is gliding the distance ΔS in the period of time Δt. The velocity of glider is calculated by Eq. (15):

$$v_{dr} = v_{cur} + v_{noi} \tag{15}$$

where v_{dr} is the estimated velocity, v_{cur} is the velocity of the sea current, v_{noi} is the additional noise.

The distance ΔS is estimated by:

$$\Delta S = v_{dr} \Delta t \tag{16}$$

The position calculated by DR is:

$$x_i = x_{i-1} + \Delta S \cos\theta_i \sin\varphi_i \tag{17}$$

$$y_i = y_{i-1} + \Delta S \cos\theta_i \cos\varphi_i \tag{18}$$

$$z_i = z_{i-1} + \Delta S \sin\theta_i \tag{19}$$

where φ_i, θ_i represent heading angle and pitch angle at the moment of i; x_{i-1}, y_{i-1}, z_{i-1} represents three direction position at the moment of $i-1$, respectively; x_i, y_i, z_i represents three direction position at the moment of i, respectively.

2. Integration Scheme

The Fig. 2 illustrates the INS/DR integration scheme used in this paper. The IMU (Initial Measurement Unit) is mainly composed of a tri-axis MEMS angular rate sensor, a tri-axis acceleration sensor and a tri-axis magnetic sensor. The tilt sensor is combined with the gravity module to estimate the accelerometer drifts, and the errors of pitch and roll calculated by accelerometers are compensated. The original angular velocities of gyroscopes $[G_x \quad G_y \quad G_z]$, the original linear accelerations of accelerometers $[A_x \quad A_y \quad A_z]$ and the original magnetic induction intensities of magnetic sensors $[M_x \quad M_y \quad M_z]$ are all processed through denoising, coordinate transformation and so on. The angular velocities treated $[\omega_x \quad \omega_y \quad \omega_z]$, linear accelerations treated $[f_x \quad f_y \quad f_z]$ and magnetic intensities treated $[H_x \quad H_y \quad H_z]$ in the body coordinate are obtained. The attitude angles (heading, pitch and roll) $[\varphi \quad \theta \quad \gamma]^{INS}$ are calculated by using the attitude matrix which is determined by the angular velocities and updated quaternions. The linear velocities $[V_E \quad V_N \quad V_U]^{INS}$ are calculated by the force equation using the updated acceleration values, and then the positions $[P_E \quad P_N \quad P_U]^{INS}$ are derived by integrating velocities. The attitude angles and velocities calculated by sensors, and the velocities $[V_E \quad V_N \quad V_U]^{DR}$ estimated by DR simultaneously enter into the EKF/RK$_4$ for the optimal estimation of errors. The original outputs of attitudes and velocities are corrected by attitude errors and velocity errors estimated above. Finally, the corrected attitude angles $[\varphi \quad \theta \quad \gamma]^C$, velocities $[V_E \quad V_N \quad V_U]^C$ and positions $[P_E \quad P_N \quad P_U]^C$ are obtained.

IV. DESIGN OF THE EKF/RK$_4$ ALGORITHM

Nonlinear models considered are presented by:

$$\mathbf{X}_k = \mathrm{f}(\mathbf{X}_{k-1}, k-1) + \Gamma(\mathbf{X}_{k-1}, k-1)\mathbf{W}_{k-1} \tag{20}$$

$$\mathbf{Z}_k = \mathrm{h}(\mathbf{X}_k, k) + \mathbf{V}_{k-1} \tag{21}$$

where $\mathbf{X}_k$ is the n-dimension random variable and is also the state vector; f and h are the nonlinear functions, respectively; Γ is a noise function; $\mathbf{W}_{k-1}$ and $\mathbf{V}_{k-1}$ are the white noise time

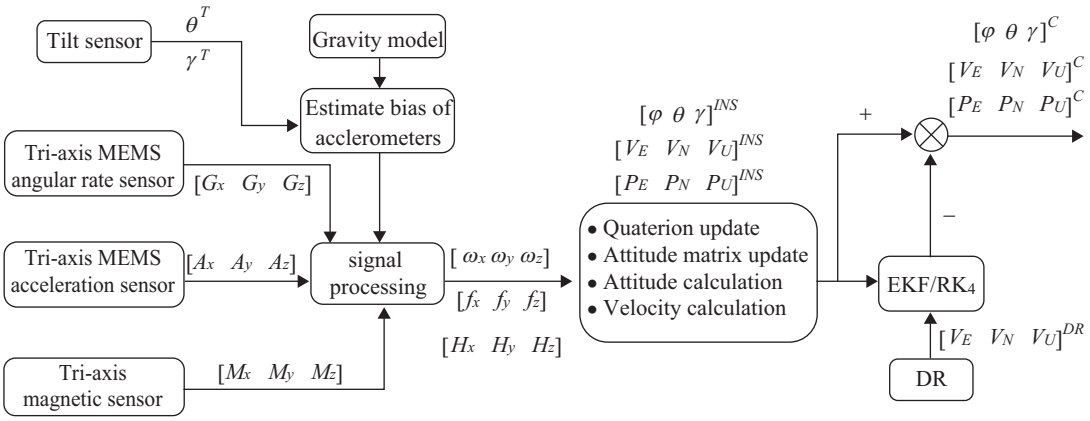

Fig. 2. INS/DR integration scheme.

series with zero mean, respectively; $\mathbf{Z}_k$ the measurement vector. Moreover, the state vector $\mathbf{X}_k$ and the measurement vector $\mathbf{Z}_k$ are given as follows:

$$\mathbf{X}_k = [\delta L \quad \delta\lambda \quad \delta h \mid \delta V_E \quad \delta V_N \quad \delta V_U \mid \phi_E \quad \phi_N \quad \phi_U \mid B_{ax} \quad B_{ay} \quad B_{az} \mid B_{gx} \quad B_{gy} \quad B_{gz}]^T \tag{22}$$

$$\mathbf{Z}_k = \begin{bmatrix} \delta\varphi \\ \delta\theta \\ \delta\gamma \\ \hline \delta V_E \\ \delta V_N \\ \delta V_U \end{bmatrix} = \begin{bmatrix} \varphi^G - \varphi^M \\ \theta^G - \theta^A \\ \gamma^G - \gamma^A \\ \hline V_E^A - V_E^{DR} \\ V_N^A - V_N^{DR} \\ V_U^A - V_U^{DR} \end{bmatrix} \tag{23}$$

where δL , $\delta\lambda$, δh represent the position errors (latitude, longitude and height) in east, north, upward directions, respectively; δV_E , δV_N , δV_U represent linear velocity errors along east, north, upward directions, respectively; ϕ_E , ϕ_N , ϕ_U are the orientation errors of the calculated platform represented in the local East-North-Upward (ENU) coordinate frame; $\delta\varphi$, $\delta\theta$, $\delta\gamma$ represent angle errors (heading, pitch and roll), respectively; φ^G , θ^G , γ^G represent heading angle, pitch angle and roll angle measured by Gyroscopes, respectively; φ^M is the heading angle measured by magnetometers; θ^A , γ^A represent pitch angle and roll angle measured by accelerometers, respectively; V_E^A , V_N^A , V_U^A represent velocity errors measured by accelerometers along three dimensions; V_E^{DR} , V_N^{DR} , V_U^{DR} represent velocity error calculated by DR along three dimensions.

The state estimation is predicted in the form:

$$\hat{\mathbf{X}}_{k|k} = \hat{\mathbf{X}}_{k|k-1} + \mathbf{K}_k(\mathbf{Z}_k - \hat{\mathbf{Z}}_k) \tag{24}$$

The estimate $\hat{\mathbf{X}}_{k|k-1}$ is determined from:

$$\hat{\mathbf{X}}_{k|k-1} = \hat{\mathbf{X}}_{k-1|k-1} + \int_{t_{k-1}}^{t_k} \mathrm{f}(\hat{\mathbf{X}}_{k-1|k-1}, \mathbf{u}_{k-1})dt \tag{25}$$

Assume

$$\mathrm{g}_{k-1}(\hat{\mathbf{X}}, \mathbf{u}) = \int_{t_{k-1}}^{t_k} \mathrm{f}(\hat{\mathbf{X}}_{k-1|k-1}, \mathbf{u}_{k-1})dt \tag{26}$$

Then

$$\dot{\mathrm{g}}_{k-1}(\hat{\mathbf{X}}, \mathbf{u}) = \mathrm{f}(\hat{\mathbf{X}}_{k-1|k-1}, \mathbf{u}_{k-1}) \tag{27}$$

For $i = 1$ to $i = \widehat{N}$

$$\mathrm{g}_{k-1}^{i+1}(\hat{\mathbf{X}}, \mathbf{u}) = \mathrm{g}_{k-1}^{i}(\hat{\mathbf{X}}, \mathbf{u}) + \frac{\tilde{\mathbf{h}}}{6}(k_1 + 2k_2 + 2k_3 + k_4) \tag{28}$$

$$k_1 = \mathrm{f}(\hat{\mathbf{X}}_{k-1}^i, \mathbf{u}_{k-1}^i) \tag{29}$$

$$k_2 = \mathrm{f}(\hat{\mathbf{X}}_{k-1}^i + \frac{1}{2}\tilde{\mathbf{h}}, \mathbf{u}_{k-1}^i + \frac{1}{2}k_1\tilde{\mathbf{h}}) \tag{30}$$

$$k_3 = \mathrm{f}(\hat{\mathbf{X}}_{k-1}^i + \frac{1}{2}\tilde{\mathbf{h}}, \mathbf{u}_{k-1}^i + \frac{1}{2}k_2\tilde{\mathbf{h}}) \tag{31}$$

$$k_4 = \mathrm{f}(\hat{\mathbf{X}}_{k-1}^i + \tilde{\mathbf{h}}, \mathbf{u}_{k-1}^i + k_3\tilde{\mathbf{h}}) \tag{32}$$

End

where the sample period $\tilde{\mathbf{h}} = \hat{\mathbf{X}}_{k-1}^{i+1} - \hat{\mathbf{X}}_{k-1}^i$ is defined; the sample range is limited in $(\hat{\mathbf{X}}_{k|k-1}, \hat{\mathbf{X}}_{k-1|k-1})$; $\widehat{N}$ is adjusted to change the sample number according to actual needs for accuracy.

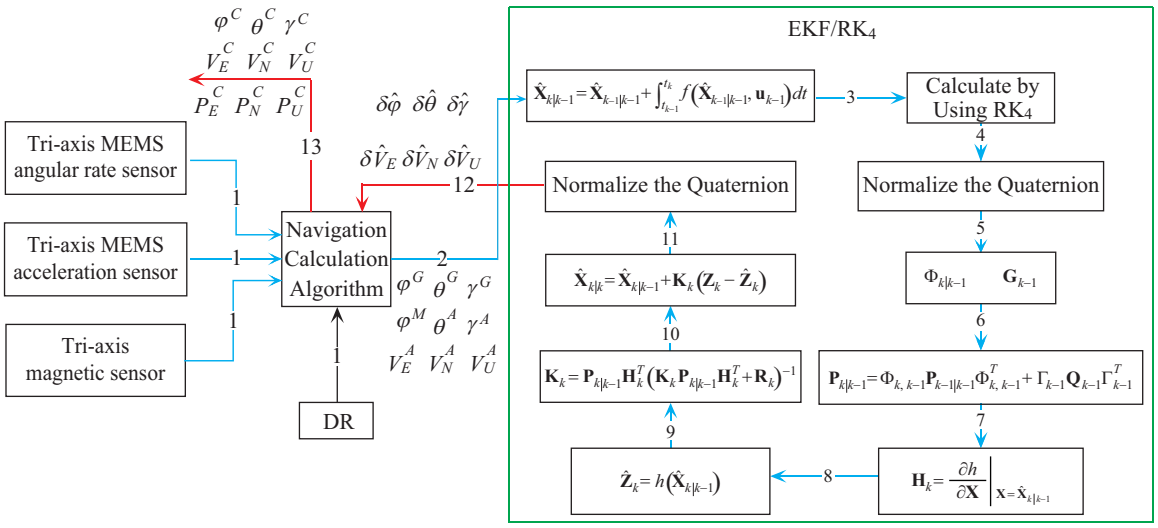

Fig. 3. The schematic diagram of EKF/RK$_4$.

The predicted output $\hat{\mathbf{Z}}_k$ is found from

$$\hat{\mathbf{Z}}_k = \mathrm{h}(\hat{\mathbf{X}}_{k|k-1}) \tag{33}$$

The gain $\mathbf{K}_k$ is obtained from

$$\mathbf{K}_k = \mathbf{P}_{k|k-1}\mathbf{H}_k^T(\mathbf{H}_k\mathbf{P}_{k|k-1}\mathbf{H}_k^T + \mathbf{R}_k)^{-1} \tag{34}$$

where $\mathbf{H}_k$ is measurement matrix and is derived from (35).

$$\mathbf{H}_k = \frac{\partial \mathrm{h}}{\partial \mathbf{X}}\bigg|_{\mathbf{X}=\hat{\mathbf{X}}_{k|k-1}} \tag{35}$$

A priori covariance matrix $\mathbf{P}_{k|k-1}$ is determined from

$$\mathbf{P}_{k|k-1} = \mathbf{\Phi}_{k,k-1}\mathbf{P}_{k-1|k-1}\mathbf{\Phi}_{k,k-1}^T + \mathbf{\Gamma}_{k-1}\mathbf{Q}_{k-1}\mathbf{\Gamma}_{k-1}^T \tag{36}$$

where $\mathbf{R}_k$ is the variance matrix of system measurement noise; $\mathbf{Q}_k$ is the variance matrix of system process noise

A posteriori covariance matrix $\mathbf{P}_{k|k}$ is determined as:

$$\mathbf{P}_{k|k} = (\mathbf{I} - \mathbf{K}_k\mathbf{H}_k)\mathbf{P}_{k|k-1}(\mathbf{I} - \mathbf{K}_k\mathbf{H}_k)^T + \mathbf{K}_k\mathbf{R}_k\mathbf{K}_k^T \tag{37}$$

where $\mathbf{I}$ is the unit matrix.

The integration scheme of EKF/RK$_4$ is shown on Fig. 3. The flow of navigation information calculation is shown by blue lines and the red lines indicate the feedback and final calculation results. The data measured by navigation sensors and the information estimated by DR are simultaneously entering into the navigation module, and then the data fusion is processed in the EKF/RK$_4$ module by using attitudes (φ^G, θ^G, γ^G, φ^M, θ^A, γ^A) and velocities (V_E^A, V_N^A, V_U^A) calculated through the navigation calculation algorithm. The state estimation $\hat{\mathbf{X}}_{k|k-1}$ is calculated by RK$_4$ algorithm, and then the quaternion is normalized. The gain $\mathbf{K}_k$ is calculated in Eq. (34) by using a priori covariance matrix $\mathbf{P}_{k|k-1}$ and measurement matrix $\mathbf{H}_k$. The current state estimation $\hat{\mathbf{X}}_{k|k}$ is calculated by Eq. (24) and then the quaternion is normalized once again. The feedback is attitude error estimates ($\delta\hat{\varphi}$, $\delta\hat{\theta}$, $\delta\hat{\gamma}$) and velocity error estimates ($\delta\hat{V}_E$, $\delta\hat{V}_N$, $\delta\hat{V}_U$).

Corrections of heading φ^C, pitch θ^C and roll γ^C are done as:

$$\varphi^C = \varphi^G - \delta\hat{\varphi} \tag{38}$$

$$\theta^C = \theta^G - \delta\hat{\theta} \tag{39}$$

$$\gamma^C = \gamma^G - \delta\hat{\gamma} \tag{40}$$

Velocity components are corrected by using the estimates of velocity errors:

$$V_E^C = V_E^A - \delta\hat{V}_E \tag{41}$$

$$V_N^C = V_N^A - \delta\hat{V}_N \tag{42}$$

$$V_U^C = V_U^A - \delta\hat{V}_U \tag{43}$$

Position components (P_E^C, P_N^C, P_U^C) in three dimensions are updated by integrating corrected velocities.

Table 1. The specifications for the attitude reference system (AHRS).

Attitude	Performance		
Heading	Range	deg	0 to 360
	Static Accuracy at Normal Conditions	deg RMS	0.2
	Static Accuracy in Temperature Range	deg RMS	0.5
	Dynamic Accuracy	deg RMS	0.7
Pitch, Roll	Range	deg	–90 to + 90, –180 to + 180
	Static Accuracy at Normal Conditions	deg RMS	0.04
	Static Accuracy in Temperature Range	deg RMS	0.1
	Dynamic Accuracy	deg RMS	0.4

Table 2. The specifications for the position reference system (GPS receiver).

Autonomous Accuracy	< 2 m
Static, Fast Static Accuracy	Horizontal: 0.3 cm + 0.5 ppm*base_line_length Vertical: 0.5 cm + 0.5 ppm*base_line_length
Kinematic Accuracy	Horizontal: 1 cm + 1 ppm*base_line_length Vertical: 1.5 cm + 1.5 ppm*base_line_length
RTK (OTF) Accuracy	Horizontal: 1 cm + 1 ppm*base_line_length Vertical: 1.5 cm + 1.5 ppm*base_line_length
DGPS Accuracy	< 0.25 m Post Processing < 0.5 m Real Time

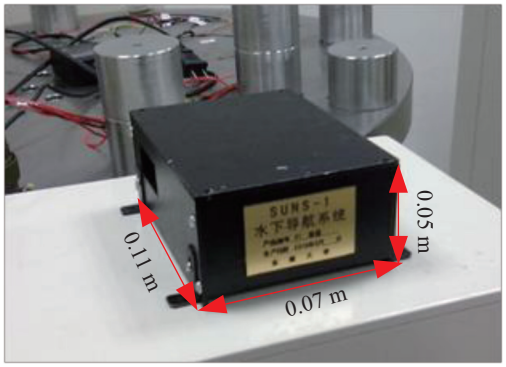

Fig. 4. The navigation system designed in our lab for the underwater glider.

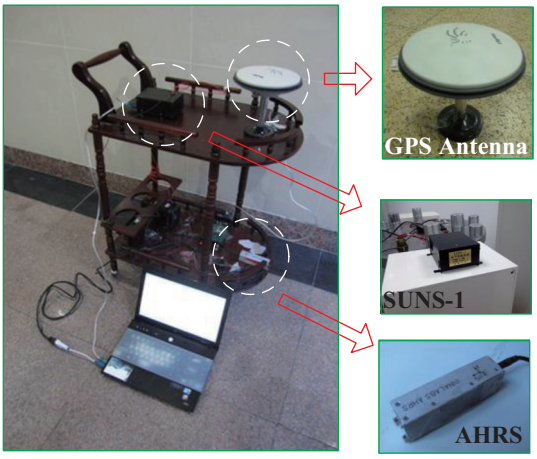

Fig. 5. The vehicle experiment.

V. EXPERIMENT AND RESULTS

1. Experiment Setup

To evaluate the performance of the proposed algorithm, a new underwater inertial navigation system is designed in our lab (Model number: SUSN-1) which is shown in Fig. 4. This system is composed of a DSP (Digital Signal Processing) unit and an IMU. The volume of this system is only 0.385 dm^3 and the power consumption is less than 0.6 w.

The AHRS (Attitude and Heading Reference System) is employed as the attitude reference and the specifications for AHRS are shown in Table 1. The GPS receiver (JAVAD GNSS) is as the position reference and the performance of GPS receiver is given in Table 2.

2. The Land Vehicle Experiment

To simulate approximately the motion of glider in the horizontal plane, the real vehicle experiments were performed on the playground of Southeast University. The vehicle with equipments is shown in Fig. 5. The trolley runs along line trajectory

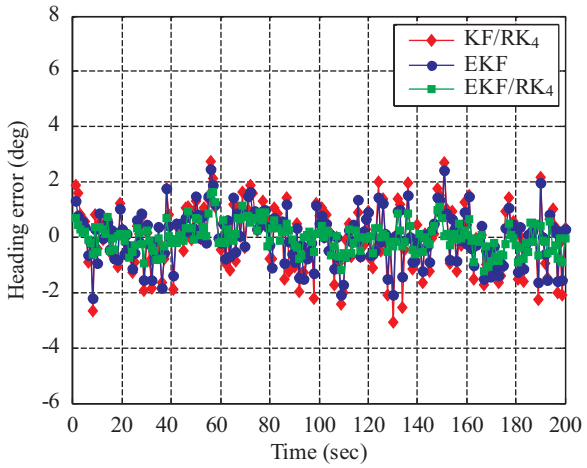

Fig. 6. Heading errors for KF/RK$_4$, EKF and EKF/RK$_4$.

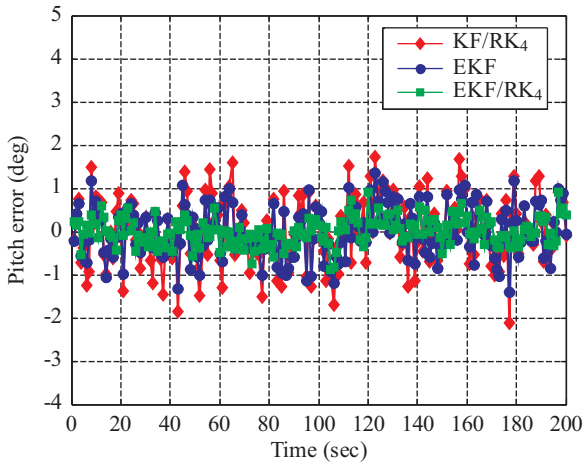

Fig. 7. Pitch errors for KF/RK$_4$, EKF and EKF/RK$_4$.

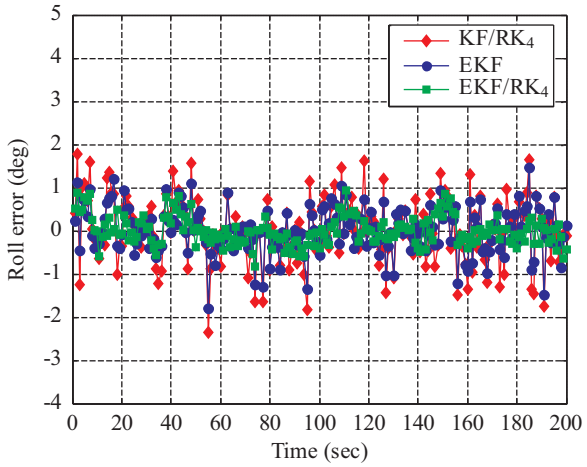

Fig. 8. Roll errors for KF/RK$_4$, EKF and EKF/RK$_4$.

and the rectangular trajectory, respectively. The velocity of the trolley is about 0.5 m/s and the sample time used in this works is 1 s.

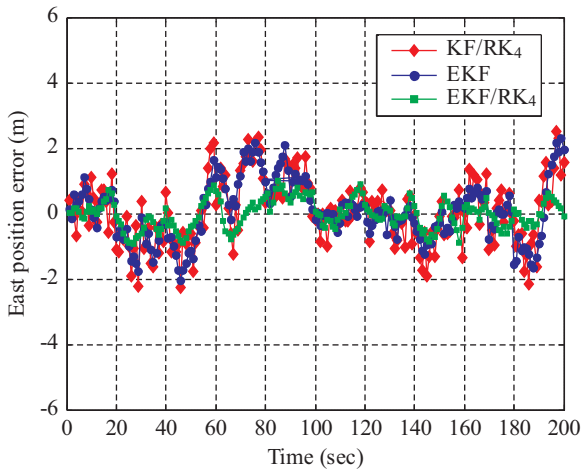

Fig. 9. East position errors for KF/RK$_4$, EKF and EKF/RK$_4$.

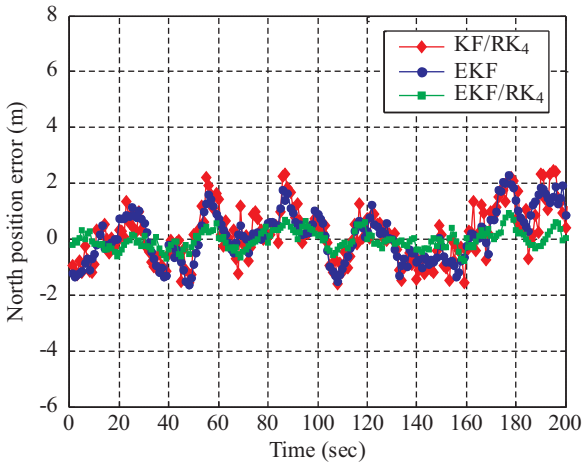

Fig. 10. North position errors for KF/RK$_4$, EKF and EKF/RK$_4$.

In the first experiment, the trolley runs along the straight line. Figs. 6-10 show the error comparison results between the propose EKF/RK$_4$ and other algorithms. The attitude angle (heading, pitch and roll) errors are shown in Figs. 6-8, respectively. The position errors in east direction and north direction are shown in Figs. 9 and 10, respectively. Furthermore, the root mean square errors (RMSE) of attitude and position for KF/RK$_4$, EKF and EKF/RK$_4$ are shown in Table 3.

From Figs. 6-10 it can be clearly seen that the performance of the proposed EKF/RK$_4$ method is much better than KF/RK$_4$ and EKF. In Table 3, we can see that, by employing the proposed EKF/RK$_4$, the RMSE of heading is reduced from 0.9779° to 0.4956°. The RMSE of pitch for EKF/RK$_4$ is 0.2945°, which is the lowest in the three algorithms. In Fig. 8, the EKF/RK$_4$ method also has the lowest error and the RMSE of roll for EKF/RK$_4$ is 0.3126°. Similarly to attitude errors, one can observe that the proposed EKF/RK$_4$ method is more effective in reducing the position error than KF/RK$_4$ and EKF. The RMSE of east position is 0.4217 m, which is lower than EKF and KF/RK$_4$.

Table 3. Comparison of errors for KF/RK$_4$, EKF and EKF/RK$_4$ (line trajectory).

	RMSE		
	KF/RK$_4$	EKF	EKF/RK$_4$
Heading (deg)	0.9779	0.9041	0.4956
Pitch (deg)	0.7334	0.5623	0.2945
Roll (deg)	0.7171	0.5251	0.3126
East position (m)	1.0649	0.9200	0.4217
North position (m)	1.0125	0.9243	0.4135

Table 4. Comparison of errors for KF/RK$_4$, EKF and EKF/RK$_4$ (rectangular trajectory).

	RMSE		
	KF/RK$_4$	EKF	EKF/RK$_4$
Heading (deg)	1.0029	0.9705	0.5067
Pitch (deg)	0.7520	0.5830	0.3073
Roll (deg)	0.7366	0.5425	0.3308
East position (m)	1.0723	0.9399	0.4703
North position (m)	1.0895	0.9461	0.4508

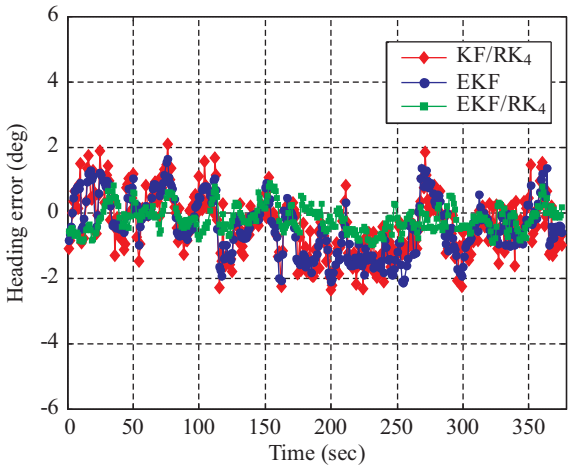

Fig. 11. Heading errors for KF/RK$_4$, EKF and EKF/RK$_4$.

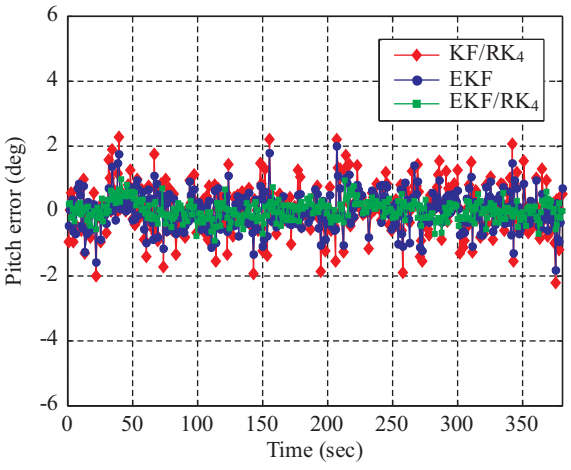

Fig. 12. Pitch errors for KF/RK$_4$, EKF and EKF/RK$_4$.

The RMSE of position for EKF/RK$_4$ in the north direction is reduced from the highest 1.0125 m to 0.4135 m.

In the second experiment, the trolley runs along the rectangular trajectory. The error comparison results for KF/RK$_4$, EKF and EKF/RK$_4$ are shown in Figs. 11-15. Figs. 11-13 show that the attitude angle (heading, pitch and roll) errors, respectively. The east error and north position error are shown in Figs. 14 and 15, respectively. The RMSE of attitude and position for KF/RK$_4$, EKF and EKF/RK$_4$ are shown in Table 4.

From Figs. 11-15, it can be concluded that the estimation accuracy in terms of attitude and position for EKF/RK$_4$ is superior to that for KF/RK$_4$ and EKF. In Table 4, by employing the proposed EKF/RK$_4$, the RMSE of heading for EKF/RK$_4$ is 0.5067°, which is lower than KF/RK$_4$ and EKF. In Fig. 12, the EKF/RK$_4$ method has the lowest pitch error and the RMSE of pitch for EKF/RK$_4$ is 0.3073°. The RMSE of roll for EKF/RK$_4$ is 0.3308°, which is the lowest compared with KF/RK$_4$ and EKF. The RMSE of east position is reduced from 1.0723 m to 0.4703 m and the RMSE of north position is reduced from 1.0895 m to 0.4508 m.

As can be seen from the real vehicle experiment, the EKF/RK$_4$ is the most effective method to reduce the attitude and position error compared with KF/RK$_4$ and EKF. KF is a popular data fusion algorithm in handling optimal estimation problems which has been widely investigated in attitude and position determination. However, the optimality of KF highly depends on the data linearity. KF/RK$_4$ is still based on the frame of KF, thus KF/RK$_4$ performs poor in the practical nonlinear system. The RK$_4$ is integrated into the EKF method in this paper. When the nonlinearity of system is not serious, the proposed EKF/RK$_4$ can make use of EKF to achieve the optimal estimation of attitude and position, and then use the RK$_4$ to improve further the estimation accuracy. Therefore, EKF/RK$_4$ performs better than EKF used alone in the practical application.

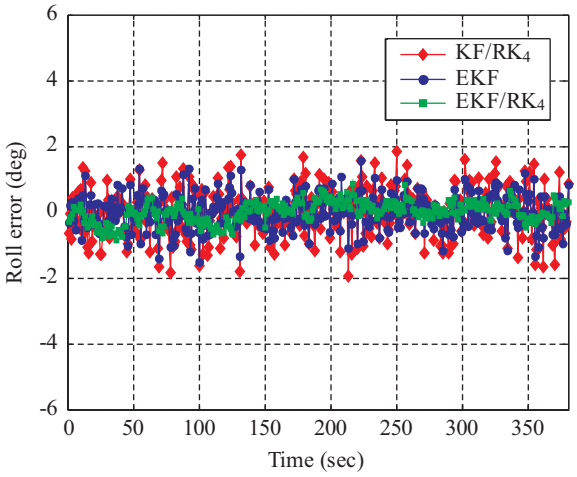

Fig. 13. Roll errors for KF/RK$_4$, EKF and EKF/RK$_4$.

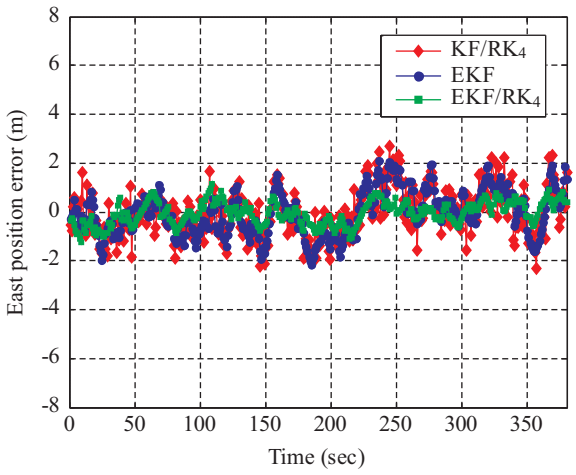

Fig. 14. East position errors for KF/RK$_4$, EKF and EKF/RK$_4$.

VI. CONCLUSION

The purpose of this paper is to develop a novel underwater navigation system which can be applied to underwater gliders in order to improve their attitude and position accuracy when GPS signal is absent underwater. This paper proposes a new underwater navigation system which is composed of inertial sensors aided by the magnetometer, and proposes the design and implementation of EKF/RK$_4$ algorithm on INS/DR integration navigation system. When the nonlinearity of system is not too serious, the proposed EKF/RK$_4$ algorithm makes better use of the advantages of EKF and RK$_4$ to improve the estimation accuracy of attitude and position. The land vehicle experiments have been done to assess the performance of the proposed EKF/RK$_4$ algorithm. The proposed EKF/RK$_4$ is a more effective and more practical method to determine the navigation information than the traditional methods and to give the optimal state estimation.

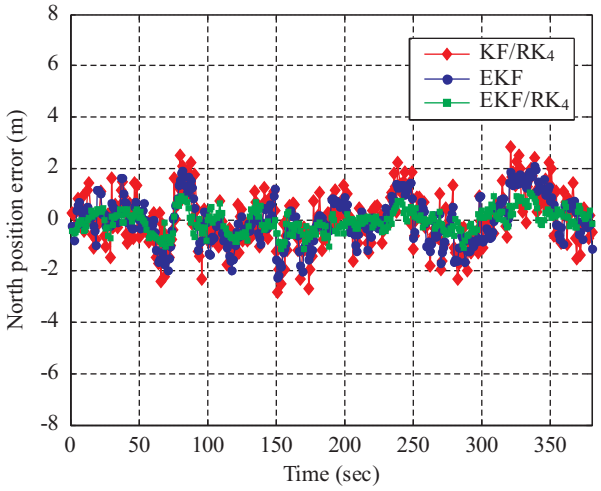

Fig. 15. North position errors for KF/RK$_4$, EKF and EKF/RK$_4$.

ACKNOWLEDGMENTS

This work is supported by Natural Science Foundation of Jiangsu Province (No. BK20160699), Jiangsu Planned Projects for Postdoctoral Research Funds (No. 1601155C), Fundamental Research Funds for the Central universities (No. 2242016R20024), Public Science and Technology Research Funds Projects of Ocean (No. 201205035).

REFERENCE

Alam, K., R. Tapabrata and S. G. Anavatti (2014). Design and construction of an autonomous underwater vehicle. Neurocomputing 142, 16-29.

Asher, B., D. M. Steinberg, A. L. Friedman and S. B. Williams (2008). Analysis of an autonomous underwater glider. Proceedings of the Australasian Conference on Robotics and Automation, Australia, 1-10.

Aydemir, G. A. and A. Saranlı (2012). Characterization and calibration of MEMS inertial sensors for state and parameter estimation applications. Measurement 45(5), 1210-1225.

Bijker, J. and W. Steyn (2008). Kalman filter configurations for a low-cost loosely integrated inertial navigation system on an airship. Control Engineering Practice 16, 1509-1518.

Cao, S. Y. and L. Guo (2012). Multi-objective robust initial alignment algorithm for Inertial Navigation System with multiple disturbances. Aerospace Science and Technology 21(4), 1-6.

Chiang, K. W., T. T. Duong, J. K. Liao, J. C. Lai, C. C. Chang, J. M. Cai and S. C. Huang (2012). On-line smoothing for an integrated navigation system with low-cost MEMS inertial sensors. Sensors 12, 17372-17389.

Chen, X. Y., C. Shen, W. B. Zhang, M. Tomizuka, Y. Xu and K. Chiu (2013). Novel hybrid of strong tracking Kalman filter and wavelet neural network for GPS/INS during GPS outages. Measurement 46, 3847-3854.

Chen X. Y., C. Shen and Y. F. Zhao (2013). Study on GPS/INS system using novel filtering methods for vessel attitude determination. Mathematical Problems in Engineering 2013, Article ID 678943, 8 pages.

Chiang, K. W., T. T. Duong and J. K. Liao (2013). The performance analysis of a real-time integrated INS/GPS vehicle navigation system with abnormal GPS measurement elimination. Sensors 13, 10599-10622.

Chu, H. J., G. J. Tsai, K. W. Chiang and T. T. Duong (2013). GPS/MEMS INS data fusion and map matching in urban areas. Sensors 13(9), 11280-11288.

Eriksen, C. C., T. J. Osse, R. D. Light, T. Wen, T. W. Lehman, P. L. Sabin, J. W. Ballard and A. M. Chiodi (2001). Seaglider: A long-range autonomous underwater vehicle for oceanographic research. IEEE Journal of Oceanic

Engineering 26(4), 424-436.

Frogerais, P., J. J. Bellanger and L. Senhadji (2012). Various ways to compute the continuous-discrete extended Kalman filter. IEEE Transactions on Automatic Control 57(4), 1000-1004.

Grewal, M. S., L. R. Weill and A. P. Andrews (2007). Global positioning systems, Inertial Navigation and Integration, 2nd ed. Wiley-Interscience.

Grewal, M. S. and A. P. Andrews (2008). Kalman Filtering: Theory and practice using MATLAB, 2nd ed. Wiley-Interscience.

Hegrenæs, Ø. and O. Hallingstad (2011). Model-Aided INS with sea current estimation for robust underwater navigation, model-aided INS with sea current estimation for robust underwater navigation. IEEE Journal of Oceanic Engineering 36(2), 316-337.

Hussain, N. A. A., M. R. Arshad and R. Mohd-Mokhtar (2011). Underwater glider modelling and analysis for net buoyancy, depth and pitch angle control. Ocean Engineering 38, 1782-1791.

Joseph, J. and J. LaViola (2003). A comparison of unscented and extended Kalman filtering for estimating quaternion motion. Proceedings of American Control Conference USA, 2435-2440.

Jwo, D. J. and T. S. Cho (2010). Critical remarks on the linearised and extended Kalman filters with geodetic navigation examples. Measurement 43(9), 1077-1089.

Jwo, D. J, J. H. Shin, C. S. Hsu and K. L. Yu (2014). Development of a strapdown inertial navigation system simulation platform. Journal of Marine Science and Technology 22(3), 381-391.

Jwo, D. J., M. Y. Hsieh and S. Y. Lai (2010). GPS navigation processing using the quaternion-based divided difference filter. GPS Solutions 14(3), 217-228.

Kondoa, H. and T. Ura (2004). Navigation of an AUV for investigation of underwater structures. Control Engineering Practice 12(12), 1551-1559.

Kandepu, R., B. Foss and L. Imsland (2008). Applying the unscented Kalman filter for nonlinear state estimation. Journal of Process Control 18(7-8), 753-768.

Lee, P. M., B. H. Jun, K. Kim, J. H. Lee, T. Aoki and T. Hyakudome (2007). Simulation of an inertial acoustic navigation system with range aiding for an autonomous underwater vehicle. IEEE Journal of Oceanic Engineering 32(2), 327-345.

Li, Y., Y. J. Pang, Y. Q. Jiang and P. Y. Chen (2011). Application of strong tracking kalman filter in dead reckoning of underwater vehicle. Electrical Engineering and Control, Lecture Notes in Electrical Engineering 98, 909-915.

Mazzoni, T. (2007). Computational aspects of continuous-discrete extended Kalman-filtering. Computational Statistics 23(4), 519-539.

Petkov, P. and T. Slavov (2010). Stochastic modeling of MEMS inertial sensors. Cybernetics and Information Technologies 10(2), 31-40.

Semeniuk, L. and A. Noureldin (2006). Bridging GPS outages using neural network estimates of INS position and velocity errors. Measurement Science and Technology 17, 2783-2798.

Shen, S. C., C. J. Chen and H. J. Huang (2010). A new calibration method for low cost MEMS inertial sensor module. Journal of Marine Science and Technology 18(6), 819-824.

Singer, H. (2005). Continuous-discrete unscented Kalman filtering, Fern Universitat, Hagen, Germany, Tech. Rep. 384.

Stancić, R. and S. Graovac (2010). The integration of strap-down INS and GPS based on adaptive error damping. Robotics and Autonomous Systems 58(10), 1117-1129.

Shen, Z., J. Georgy, M. J. Korenberg and A. Noureldin (2011). Low cost two dimension navigation using an augmented Kalman filter/Fast Orthogonal Search module for the integration of reduced inertial sensor system and Global Positioning System. Transportation Research Part C: Emerging Technologies 19(6), 1111-1132.

Slavov, T. and P. Petkov (2011). Strapdown inertial system based on improved MEMS error models. Cybernetics and Information Technologies 11(4), 3-23.

Sun, B., D. Q. Zhu, F. Ding and S. X. Yang (2013). A novel tracking control approach for unmanned underwater vehicles based on bio-inspired neurodynamics. Journal of Marine Science and Technology (Japan) 18(1), 63-74.

Tang, M. Q., Z. Q. Zhang and Y. Q. Xing (2011). Analysis of new developments and key technologies of autonomous underwater vehicle in marine survey. Procedia Environmental Sciences 10, 1992-1997.

Wang, X. Y. and Y. Huang (2011). Convergence Study in Extended Kalman Filter-Based Training of Recurrent Neural Networks. IEEE Transaction on Neural Networks 22(4), 588-600.

Wilkie, J. (2004). Numerical methods for stochastic differential equations. Physical Review E 70(1), 1-4.

Zhu, D. Q. and Y. Zhao (2011). A bio-inspired dynamic path-following control of autonomous underwater vehicle. Proceedings of the 16th IASTED International Conference on Robotics and Applications, Robotics and Applications with Symposia 739: Computational Photography and 740: Computer Vision, Vancouver, BC, Canada, 22-29.

Zhang, T. and X. S. Xu (2012). A new method of seamless land navigation for GPS/INS integrated system. Measurement 45(4), 691-701.

Zhang, S. W., J. C. Yu, A. Q. Zhang and F. M. Zhang (2013). Spiraling motion of underwater gliders: Modeling, analysis, and experimental results. Ocean Engineering 60, 1-13.